

Mapping the optical properties of slab-type two-dimensional photonic crystal waveguides

Eric Dulkeith,* Sharee J. McNab, and Yurii A. Vlasov
IBM T. J. Watson Research Center, Yorktown Heights, NY 10598, USA
 (Dated: November 9, 2018)

We report on systematic experimental mapping of the transmission properties of two-dimensional silicon-on-insulator photonic crystal waveguides for a broad range of hole radii, slab thicknesses and waveguide lengths for both TE and TM polarizations. Detailed analysis of numerous spectral features allows a direct comparison of experimental data with 3D plane wave and finite-difference time-domain calculations. We find, counter-intuitively, that the bandwidth for low-loss propagation completely vanishes for structural parameters where the photonic band gap is maximized. Our results demonstrate that, in order to maximize the bandwidth of low-loss waveguiding, the hole radius must be significantly reduced. While the photonic band gap considerably narrows, the bandwidth of low-loss propagation in PhC waveguides is increased up to 125nm with losses as low as 8 ± 2 dB/cm.

I. INTRODUCTION

Two-dimensional photonic crystals (PhC) have gained considerable interest and are regarded as a promising platform for dense integration of planar photonic integrated circuits on a chip-scale level [1, 2, 3, 4, 5, 6, 7, 8, 9, 10, 11, 12, 13, 14, 15, 16, 17, 18, 19]. In particular, PhCs fabricated on silicon-on-insulator (SOI) provide waveguide cross-sectional areas on the sub-micron scale while maintaining single-mode operation due to high refractive index contrast [4, 5, 6, 7, 8, 9, 10, 11, 12, 13, 14]. It has been shown that for triangular lattice membrane-type PhCs [15, 16, 17], consisting of a periodic array of holes with a silicon slab thickness h around $0.5a$ and hole radii of $\sim 0.35a$ (a is the lattice constant) the bandwidth of the photonic band gap (PBG) can extend over most of the 1.3 and $1.5\mu\text{m}$ telecommunications transmission bands. Single-mode waveguiding can be realized by removing a single row of holes in the periodic photonic lattice along the Γ -K direction [16, 17]. Mode confinement within the silicon slab in the vertical direction is accomplished by index guiding, while lateral confinement within the slab plane is defined by the PBG [18]. This hybrid confinement limits the bandwidth for intrinsically loss-less propagation to frequencies that are below the light line cutoff. Above the light line cutoff the propagation becomes lossy with mode-leakage out of the slab [6, 10]. Consequently, the bandwidth for intrinsically low-loss propagation (LLP) of the waveguiding mode is restricted to only a fraction of the PBG, e.g. in the order of only a few tens of nanometers [7, 8, 9, 10, 13, 14]. These insights and many other theoretical investigations of light confinement in planar PhCs and PhC waveguides have been examined in detail and are well understood. In contrast, experimental studies of the waveguiding properties of the slab-type PhC waveguides have been hindered for a long time by difficulties in fabricating these structures. One

of the major challenges in the last decade was to overcome extremely high transmission losses due to surface roughness, structural irregularities and inefficient coupling, which significantly complicated the interpretation of experimental results. Recent achievements in optimizing the light coupling efficiency into the PhC as well as fabrication improvements reducing surface roughness have led to ultra low-loss PhC waveguides thus enabling further spectroscopic exploration [10, 11, 13, 14].

In this paper, we present detailed and comprehensive experimental studies of the transmission properties of TE-like (even parity with respect to the slab plane) and TM-like (odd parity with respect to the slab plane) modes of two-dimensional membrane-type PhC waveguides. The spectral properties are measured as a function of various lattice parameters such as hole radius r , slab thickness h , and the crystal length l . A survey of the applied experimental techniques, fabrications methods and theoretical calculations is given in Sec. II. In Sec. III we explore the transmission properties of the PhC waveguides with structural parameters optimized for a maximum bandgap. We show that for large hole radii of $r/a \sim 0.38$ the bandwidth for LLP completely disappears due to effective interaction with the band edge slab modes of the PhC. The transmission properties of PhC waveguides with small hole radii spanning from $r/a=0.22$ - 0.34 are investigated in Sec. IV. We find, counter intuitively, that in order to maximize the bandwidth of the waveguiding mode the hole radius needs to be reduced to $r/a \sim 0.2$. Although this optimization is accompanied by a significant decrease of the PBG, the bandwidth for propagation is increased up to 125nm, maintaining a reasonable trade-off between bandgap and propagation bandwidth. The experimental findings are compared to 3D planewave calculations using the MIT Photonic Band code [19] and 3D-Finite Difference Time Domain (FDTD) [20]. For the propagation bandwidth-optimized parameters, we deter-

mine losses as small as $8\pm 2\text{dB/cm}$, which is one of the lowest reported to date. Sec. V. will deal with experimental results of transmission spectra in TM polarization. After their comparison with photonic band structures, in Sec. VI we will address the observed coupling of even TE- with odd TE- and TM-like modes. Results are summarized in Sec. VII.

II. EXPERIMENTAL

Devices were fabricated on lightly p-doped 200mm silicon-on-insulator SOI wafers from SOITEC [24] with a Si device layer thickness h of 220nm on top of a $2\mu\text{m}$ buried oxide layer (BOX). The processing is performed on a standard CMOS fab line at the IBM Watson Research Center as described elsewhere [10, 11]. A 50nm thick oxide is deposited via chemical vapor deposition to serve as a hard mask for etching. The wafers are patterned by electron beam lithography (LEICA-VB6, 100keV, single writing field $400\mu\text{m}$). The oxide hard mask is opened and the silicon device layer dry is etched $CF_4/CHF_3/Ar$ and HBr chemistry, respectively. After structure definition the BOX layer is selectively under-etched in a buffered HF to form suspended membranes. PhC waveguides are defined by omitting one row of holes from the PhC lattice in the $\Gamma - K$ direction (W1-type waveguide). The light is coupled to the PhC waveguide via a butt-coupled single-mode strip waveguide. After definition of the PhC membrane the polymer inverted spot-size converters are fabricated to achieve high coupling efficiency as reported elsewhere [10, 11]. Three different wafers with slightly different slab thicknesses h were processed with PhC waveguides having nominally the same lattice constant $a=437.5\text{nm}$, but different hole radii $r=96, 140$ and 165nm ($r/a=0.22, 0.32$, and 0.35 , respectively). The PhC waveguide length is varied in each writing field from $29\mu\text{m}$ to $2000\mu\text{m}$ for accurate loss determination. Four of such fields grouped together constitute one experimental chip with the e-beam exposure dose intentionally varied between each field. This allows the phase space of explored lattice parameters to be further broadened. In addition, proximity effects due to background electron beam scattering induce further minor changes in the hole diameter between the different PhC waveguides even within one field. Such variation allows the exploration of a quasi-continuous range of different lattice parameters, but at the same time requires thorough statistical analysis of the particular PhC waveguide on a given chip.

The lattice constant a , Si slab thickness h , and the hole radii r on a given sample are determined by statistical evaluation of a number of SEM images obtained on a LEO SEM1560 model with identical imaging conditions (acceleration voltage, focal distance, magnification, column and aperture alignment, etc). Over 110

PhC waveguides were characterized in total. The lattice constant was measured four times for each PhC waveguide (total number of measurements $N=440$) yielding an overall value of $a=437.6\text{nm}$ with a standard deviation of only $\sigma=0.93\text{nm}$.

In order to check the variation of the hole radius along a single PhC waveguide $N=60$ holes were measured at three different locations along the longest $2000\mu\text{m}$ -long waveguide separated by approximately $600\mu\text{m}$. The results yield statistically identical mean hole radii of 99.21nm at one end of the PhC waveguide, 99.18nm in the middle section, and 98.17nm at the other end with standard deviations not exceeding 1.2nm . The overall mean hole radius for the total of $N=180$ measurements was found to be 98.9nm with $\sigma=1.12\text{nm}$. For all other PhC waveguides the hole radius was measured only six times in their middle section. Although this small number imposes a less accurate estimation of the mean value, however from the of $N=180$ measurements the resulting standard error does not exceed 0.5% for $N=6$. The slab thickness h of the wafers was measured at nine different positions along each sample. For the three processed SOI wafers with devices having $r/a=0.22, 0.32$ and 0.35 the normalized thickness of the Si slab was measured to be $h/a=0.518, 0.507$ and 0.546 respectively.

Measurements of transmission spectra of PhC waveguides are performed using a broadband (1200-1700nm) LED source and an optical spectrum analyzer (OSA) with 5nm spectral resolution. A rejection ratio of over 30dB between TE and TM polarizations is achieved with the use of polarization maintaining, tapered and lensed fibers and a polarization controller. The transmission spectra of the PhC waveguides are normalized to the transmission spectra of a corresponding single-mode reference strip waveguides located in the same writing field near the PhC structures as described elsewhere [10, 11].

The experimental results are compared with 3D plane wave calculations performed using the MIT Photonic-Band code [19]. The dielectric permittivity ϵ_{Si} of the Si slab and ϵ_{SiO_2} of the oxide layer are taken as 12.1 and 2.0 , respectively. Values for the hole radii and lattice constant are chosen as determined by SEM measurements. The grid resolution (number of vectors in the unit cell of the PhC) of the plane wave calculations is set to $16\times 16\times 16$, which gives an error in the eigenvalue convergence below $\sim 2\%$ with reasonable calculation time [19]. However, the limited resolution imposes a drawback that very small changes in the slab thickness h are not well resolved especially for the TE-like modes resulting in a step-like rather than a smooth dependence of the calculated band structures on h . To overcome this issue, the photonic crystal band structures for slab thicknesses with $h/a=0.4, 0.5, 0.6$ and 0.7 are calculated and intermediate values are interpolated. Interestingly, to achieve the best agreement between experiment and theory all slab thicknesses needed to be assumed $5\text{-}10\%$ thinner than

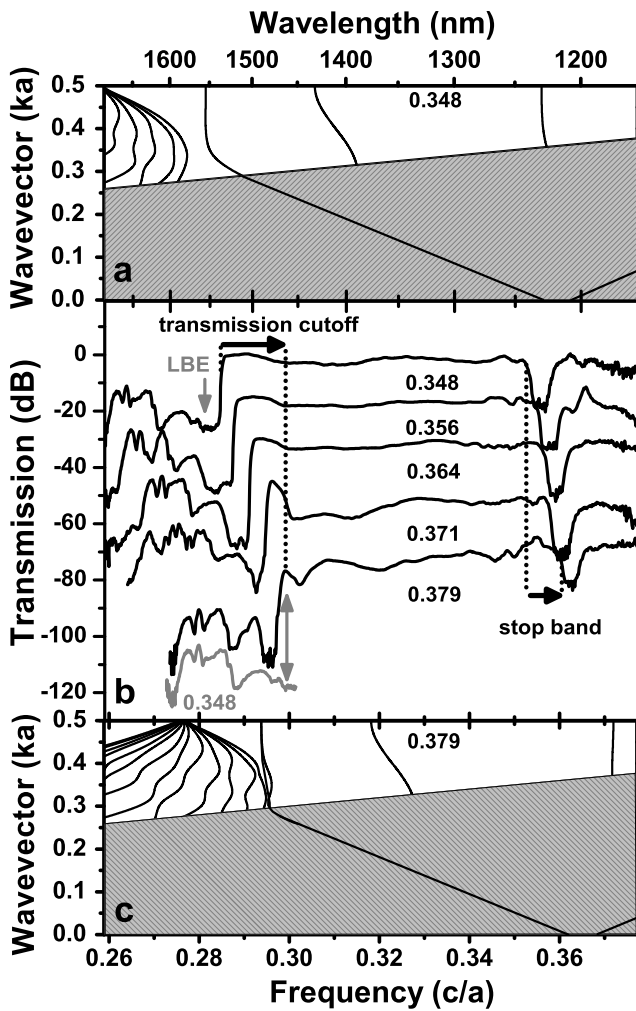


FIG. 1: Comparison of experimental TE transmission spectra of PhC waveguides with large hole radii against 3D plane wave band structure calculations. a) Band structure for a PhC waveguide with a hole radius of $r/a=0.348$. b) Set of transmission spectra for PhC waveguides, equal in length ($l=29\mu\text{m}$) but with increasing hole radius $r/a=0.348-0.379$. The grey curve illustrates the spectral merge of LBE and waveguiding onset for the PhC with $r/a=0.379$ (slab modes for $r/a=0.348$ shifted with respect to the normalized frequency for comparison with the modes for $r/a=0.379$). c) Band structure for a PhC waveguide with a hole radius of $r/a=0.379$.

measured by SEM. This discrepancy is consistent with a small, but noticeable thinning of the silicon slab in the membrane region during the BOX etch.

All calculations of transmission spectra are performed with a 3D finite difference time domain method (3D FDTD) using the Fullwave software package [20]. Transmission through a 33 unit cell long PhC W1 waveguide with 13 rows of holes on each side is calculated with a $265 \times 243 \times 551$ mesh (20nm grid size) for over 250000 time steps.

III. PHC WAVEGUIDES WITH MAXIMIZED PHOTONIC BANDGAP (TE-LIKE MODES)

Historically most efforts on both three-dimensional and two-dimensional PhCs, were focused on maximizing the bandwidth of the PBG [15]. A large variety of different hole shapes and crystal symmetries were explored in a planar 2D geometry. It was shown [15] that for a 2D PhCs a triangular lattice of air holes (hexagonal first Brillouin zone), produces the widest PBG for a slab thickness of $\sim 0.5a$ and hole radii of $\sim 0.35a$. Waveguiding can then be provided by omitting a row of holes or increasing the hole radius in the channel. It is known however, that the resulting mode suffers from light leakage out of the plane for frequencies above the light line. Leakage losses were measured [6, 10] to be as high as 1500dB/cm, which prohibits utilization of this wavelength range for useful waveguiding. These inevitable diffraction losses limit the bandwidth for intrinsic low-loss propagation (LLP) below the light line to only a fraction of the PBG [7, 8, 9, 10, 13, 14]. Sec. III will first report on the transmission properties of triangular 2D PhC waveguides as a function of the hole radius that are chosen to match the conditions for an optimized PBG ($r/a=0.348-0.384$).

Figure 1 shows a series of transmission spectra of PhC waveguides of identical length ($29\mu\text{m}$), but different hole radii and compares them with photonic band structure calculations. A number of spectral features of the TE-like modes can be directly mapped to the band diagram. Figure 1a presents the photonic band structure for the PhC waveguide with the smallest radius of $r/a=0.348$. The onset of the waveguiding mode at wavelengths around 1550nm, also known as the mode gap cutoff [7, 8], is clearly seen. In the corresponding measured spectrum, this onset results in a sharp transmission cutoff around 1535nm (Fig.1b, upper curve). The bandwidth for intrinsic LLP is strictly bounded by this and the crossing of the waveguide mode with the light line. Calculations show the light line cutoff is at $\sim 1510\text{nm}$ (normalized frequency of $0.29c/a$). Since the length of the PhC waveguide is only 60 unit cells, the light line cutoff manifests itself as only a weak kink at $\sim 1505\text{nm}$ in the experimental spectra. The LLP bandwidth can be determined to be $\sim 30\text{nm}$. At longer wavelengths, small resonances are present in the measured transmission spectrum. According to the photonic band structure, these resonances are identified as a series of slab modes below the lower photonic band edge (LBE). These modes are delocalized over the whole slab with their fields mainly concentrated in the dielectric material (dielectric bands) [15, 16]. At shorter wavelengths, around 1230nm, the transmission reveals a distinct stop band. This stop band opens due to the folding of the waveguiding mode at the edge of the Brillouin zone at $k=0$. The upper band edge (UBE), which is defined by the commencement of

slab modes that are predominately located in the holes (air bands) [15, 16], are not observed in the current set of spectra since it lies at 1110nm ($0.40c/a$), as determined by band structure calculations.

The series of transmission spectra in Fig. 1b shows that as the hole radius increases, all characteristic spectral features of the PhC waveguide undergo a shift to higher energies and is confirmed by the photonic band structure in Fig. 1c ($r/a=0.379$). This fact can be easily explained by a decrease of the effective refractive index of the slab. However, in addition, the spectral shape of the transmission in the region of LLP changes drastically. For the smallest hole radius the LLP transmission region is characterized with a nearly flat top profile. The propagation losses for waveguides with approximately the same radius were measured before as small as $24\pm 3\text{dB/cm}$. In contrast, for PhC waveguides with larger hole radii, first, the flat top profile in the vicinity of the mode onset gradually narrows and then completely disappears for $r/a=0.379$, second, propagation losses in this region can be estimated to be as high as 70dB/cm indicating the complete vanishing of the LLP for PhC waveguides for large hole radii.

Interestingly, by analyzing Fig. 1, it can be seen that with increasing hole radius the blueshift of the transmission cutoff is far more pronounced than the corresponding blueshift of the stop band. This is surprising since both stem from the same waveguiding mode. To clarify this issue the experimental results over a large number of PhC waveguides with different hole radii are summarized in Fig. 2. The spectral positions of waveguiding mode onset, stop band, light line cutoff and onset of the LBE slab modes are plotted against normalized hole radii (measured using a SEM on the very same waveguides). For this particular range of hole radii the spectral position of the light line is nearly constant. Since both, the mode onset and the stop band are defined by the same PhC waveguiding mode, a change in radius should lead to a parallel wavelength shift. The experimental results for $r/a < 0.37$ confirm this behavior. In addition, the bandwidth for LLP continuously shrinks with increasing the hole radius. On the other hand, the LBE exhibits a much steeper spectral shift since the corresponding modes are delocalized over the whole slab, thus being easily affected by even small changes in the hole radius. The PhC waveguiding mode instead is mainly localized in the center of the waveguide and is less influenced by the surrounding holes. As a result, for hole radii with $r/a > 0.37$ the experimental transmission cutoff is no longer defined by the waveguiding mode onset, but rather by the onset of the slab modes at the LBE. This causes the LLP bandwidth to completely vanish for large hole radii.

This experimental observation is confirmed by photonic band structure calculations in Fig. 1a and Fig. 1c. While for $r/a=0.348$ the waveguiding onset and the LBE are clearly spectrally separated, for $r/a=0.379$ the LBE

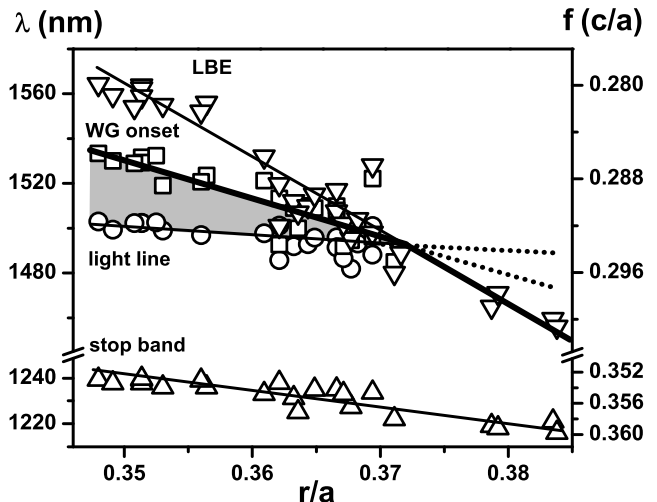


FIG. 2: Experimentally determined TE-map of spectral positions of lower band edge (LBE), waveguiding onset, light line and stop band as a function of the normalized hole radius for $r/a=0.348-0.384$. The grey shaded area shows the frequency region for low loss propagation (lines are guides for the eye).

overlaps with the waveguiding mode. Thus, light from the access strip waveguide can couple not only effectively to the PhC waveguiding mode, but also to the slab modes and hence leaks into the slab. This explains the dramatic increase of the propagation losses. For PhC waveguides with $r/a > 0.37$, it leads to a zero-bandwidth for low-loss propagation. The results presented in this section demonstrate that with structural parameters, chosen to maximize the PBG, the bandwidth for LLP finally vanishes.

IV. PHC WAVEGUIDES WITH MAXIMIZED LOW LOSS PROPAGATION BAND (TE-LIKE MODES)

Instead of optimizing the bandwidth of the PBG (a parameter rather irrelevant for the implementation of PhC waveguides in integrated optics), it is more meaningful to optimize the bandwidth of LLP. From the analysis of the previous results in Sec. III we can conclude that smaller hole radii are required for the optimization of the LLP bandwidth. In Fig. 2 we have seen that for a decrease of the hole radius of only $\sim 5\%$ ($r/a=0.365 \rightarrow 0.348$) the LLP bandwidth significantly broadens by more than a factor of two ($13 \rightarrow 30\text{nm}$). To confirm this trend, this section will first deal with PhC waveguides of only slightly smaller hole radii ($r/a=0.32-0.34$). In the second part we will then proceed to investigate PhC waveguides with very small holes ($r/a=0.22-0.24$).

The experimental transmission spectra of PhC waveguides with different lengths from 29 to $2000\mu\text{m}$ but ap-

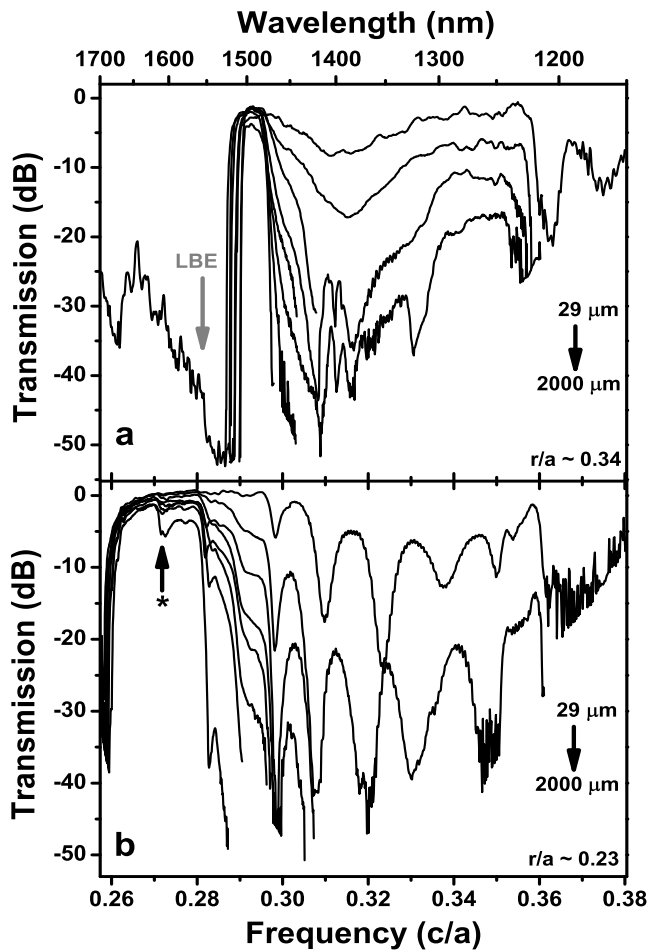


FIG. 3: Length series of TE transmission spectra of PhC waveguides (29-2000 μm) for two different hole radii: a) $r/a \sim 0.34$ and b) $r/a \sim 0.23$. The transmission dip marked with an asterisk corresponds to the x -odd TE-like mode (see text for details).

proximately the same hole radius ($r/a \sim 0.34$) are shown in Fig. 3a. In the same manner as done in Fig. 1, the comparison of transmission spectra with photonic band structure calculations (not shown) enables the identification of the spectral features of the PhC waveguides. For the waveguide length of 29 μm (upper curve), the LBE is clearly visible in the long wavelength region at 1560nm. The sharp transmission cut off, located at 1515nm corresponds to the waveguiding onset and the light line cutoff is seen at 1480nm. At shorter wavelengths, the transmission spectrum displays a stop band at 1220nm. In fact, the spectra look very similar to the results of Fig. 1b, however the PBG bandwidth is significantly reduced by 25nm, while the bandwidth for LLP increases up to 35nm. The results of Fig. 3a can be used to determine the propagation losses in the LLP region. Losses at 1500nm are calculated to be $20 \pm 3\text{dB/cm}$; the method is described later in this section (see also Ref.10).

Since the expansion of the bandwidth for LLP simultaneously takes place with a shrinking of the PBG, one can conclude that there must be a lower limit for the radius where the LLP bandwidth would be restricted by the slab modes of the UBE. To find the upper limit of the LLP bandwidth, PhC waveguides with significantly reduced hole radii need to be investigated. Fig. 3b shows the experimental results of a series of transmission spectra of PhC waveguides with different lengths but again nearly the same hole radii ($r/a \sim 0.23$). Compared to Fig. 3a, the size of the hole radius is reduced by over 30% and causes a drastic change in the transmission spectra. Within the measured spectral range, no LBE is detected, since it has redshifted to 1730nm. Furthermore, the stop band has also disappeared from the spectra. On the very edge of the transmission spectra, around 1695nm, a sharp transmission cut off is present, and for shorter wavelengths is followed by a region of flat transmission and relatively low losses. At wavelengths shorter than 1550nm, the transmission spectra are now dominated by very strong resonances covering a broad bandwidth.

To understand the origin of these resonances and to interpret the experimental transmission spectra, Fig. 4a compares the transmission spectrum of a 29 μm PhC waveguide with $r/a=0.22$ against 3D FDTD calculations. For calculations the thickness of the slab was defined as $h/a=0.52$. The FDTD calculated spectrum is in good agreement with the experimental transmission spectrum. The difference in amplitude is due to the shorter waveguide length used in the calculations (33 unit cells or 14.4 μm). The comparison of calculated and experimental transmission spectra allows identification of the measured transmission cutoff around 1700nm as the onset of the waveguiding mode, The onset is followed by numerous resonances starting at 1725nm. In direct analogy with the interpretation of the experimental results shown in Fig. 1b and Fig. 3a, these resonances can be attributed to modes below the LBE.

The calculated transmission also confirms the presence of additional resonances between 1200 and 1500nm. However, from the FDTD spectrum alone it is not possible to assign their origin. To address this issue Fig. 4b presents photonic band structure calculation consistent with the structural input parameters in Fig. 4a. The strong resonances clearly match with slab modes whose spectral onset defines the UBE. The UBE, not visible in the previous spectra of Fig1b and Fig3a for large hole radii, has now redshifted over 400nm, almost spectrally matching the position of the light line cutoff. This huge spectral shift of the UBE is far more pronounced than the shift of the LBE. As mentioned before, UBE (air)-modes are mainly located in the holes of the PhC and thus exhibit a strong dependence on hole radius. In the experimental transmission spectrum of Fig. 4a, a kink around 1570nm indicates where the waveguiding mode crosses the light line. This becomes more visible for

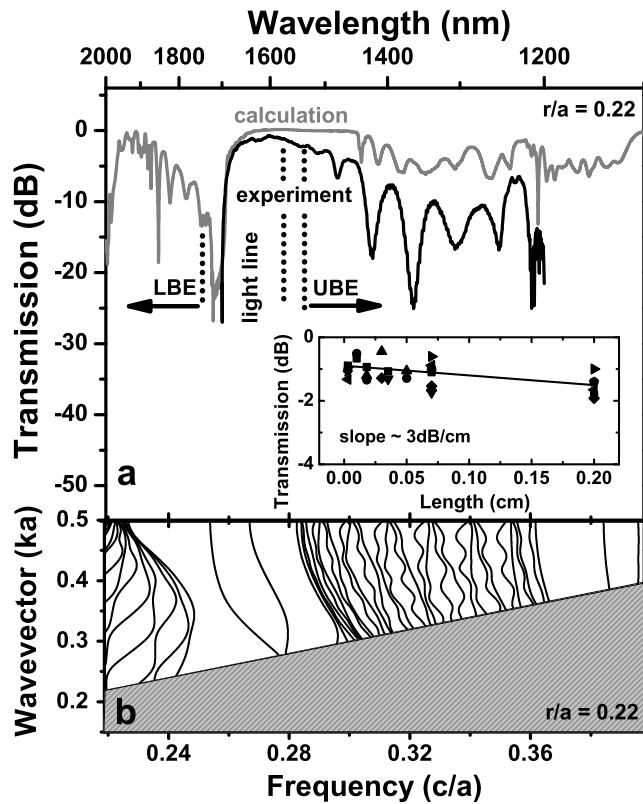


FIG. 4: a) Experimental TE transmission spectra (black line) of a $29\mu\text{m}$ PhC waveguide with $r/a=0.22$ compared with 3D FDTD calculations (grey line). Inset: Absolute transmission at 1650nm of PhC waveguides as a function of the length. From the slope, the losses of the whole photonic circuit (PhC and strip waveguides) are determined as $3\pm 2\text{dB/cm}$. This corresponds to $8\pm 2\text{dB/cm}$ loss for the PhC waveguide (see text for details). b) 3D plane wave band structure calculations with the same structural input parameters as for the FDTD calculations in a).

longer waveguide lengths as shown in Fig. 3b (note this is for $r/a\sim 0.23$). The bandwidth for LLP in Fig. 4a. is now close to 130nm , an increase of nearly 300%. This very broad bandwidth is confirmed by comparison with the corresponding photonic band structure in Fig. 4b.

Losses within the LLP band are determined from transmission spectra of PhC waveguides with different length. The inset in Fig. 4a presents the absolute transmission values measured at 1650nm . The slope of the transmission attenuation gives $3\pm 2\text{dB/cm}$. Note that this number corresponds to the total transmission losses through the PhC waveguide and access strip waveguides, rather than characterizing the losses in the PhC waveguide alone. While the length of the PhC waveguides and their corresponding losses is increasing, at the same time the length of the strip waveguides is shortened to keep the total length of the photonic circuit on a chip constant at 4.6mm . Correspondingly, as it was pointed

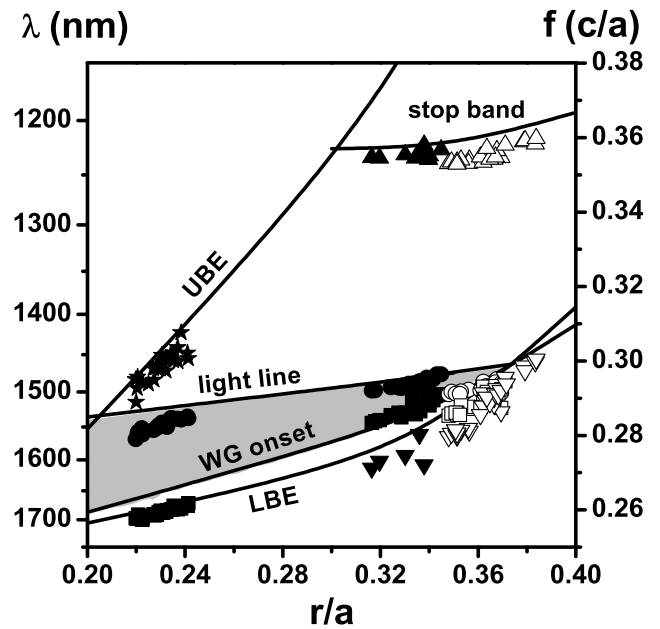


FIG. 5: Experimentally derived TE-map depicting spectral positions of stop band (triangles up), UBE (asterisks), light line (circles), WG onset (squares) and LBE (triangles down) as a function of the hole radius $r/a=0.22-0.38$. Solid lines represent 3D plane wave band structure calculations with input parameters determined from SEM measurements for hole radii with $r/a=0.32-0.34$.

out in Ref.10, for a correct determination of propagation losses in the PhC waveguide it is necessary to account for losses in the bare strip waveguide. Losses from TE-like modes in analogous strip waveguides with a $460\times 220\text{nm}$ cross-section have been determined recently as 3.6dB/cm and 5dB/cm at 1500nm and 1650nm respectively, as reported elsewhere [21]. Correspondingly, the effective loss of the PhC waveguide alone at 1650nm can be estimated as $8\pm 2\text{dB/cm}$. To our knowledge, this is one of the lowest loss numbers reported for SOI PhC waveguides. There is a remarkable dependence on the hole radius. Losses decrease from $24\pm 3\text{dB/cm}$ for $r/a=0.365$ (Ref.10) to $20\pm 3\text{dB/cm}$ for $r/a=0.34$ and to $8\pm 2\text{dB/cm}$ for $r/a=0.23$. It can be argued that the surface area of the holes is significantly decreased in the waveguides with smaller radii, thus scattering losses due to sidewall roughness are becoming less pronounced. In addition, the effective waveguide width increases with decreasing hole radius which can further reduce losses.

Figure 5 summarizes the experimental results of the PhC waveguides for all measured hole radii. The spectral positions of the TE spectra such as stop band, UBE, LBE, light line and waveguiding onset are shown as a function of the normalized hole radius (open shapes correspond to data from Fig. 2). The experimental results are compared to 3D planewave calculations (solid line)

for the slab thickness of h taken as $0.473a$. This corresponds to the hole size series ranging from $r/a=0.32-0.34$. Good agreement is found overall between experiment and calculation. The results in Fig. 5 clearly demonstrate the broadening of the bandwidth for LLP, which is accompanied by a simultaneous shrinkage of the PBG with decreasing hole radii. A closer look shows that the set of data points for the three different size series have a minor spectral displacement with respect to each other. This step-like behavior can be explained by the different slab thicknesses h of the SOI wafers as measured with a SEM (see Sec. II).

As can be seen from the planewave calculations in Fig. 5, the maximum LLP with over 150nm bandwidth is achieved for hole radii $r/a=0.207$. Here the PBG bandwidth is reduced to 160nm, however the LLP region occupies nearly 94% of the bandwidth. Apparently, further decrease of the radii would shrink the LLP bandwidth again, as the slab modes of the UBE would merge into the LLP.

V. TRANSMISSION OF THE TM-LIKE MODES IN PhC WAVEGUIDES

It is well known that a PBG for the TM-like modes does not exist for SOI PhC slabs [15]. However, it is important to characterize the transmission characteristics of PhC waveguides for TM-mode as well. Firstly, measurements of TE- and TM-like modes provide good verification and validation of theoretical fitting. With a set of only three fitting parameters (hole radius, refractive index and slab thickness) all spectral features found in both, TE- and TM-spectra, have to simultaneously match the band structure calculations. Secondly, and more importantly, due to possible imperfections and errors in the experimental structures, TM-like modes in principle may interact with the TE-like modes of interest and cause additional propagation losses [11].

Measured transmission spectra of TM-like modes are shown in Fig. 6a. The hole radius of the PhC waveguides is $r/a\sim 0.33$. The length of the different photonic crystals range from 29 to $700\mu\text{m}$. All transmission spectra exhibit a strong dip at around 1325nm, as well as multiple strong resonances starting at 1280nm and extending up to the transmission cutoff at 1235nm. As before, 3D plane wave calculations of the photonic band structure are helpful in interpretation of the spectral features (Fig. 6b). A dotted line indicates the fundamental TM-like waveguiding mode. Both in- and out-of-plane confinement of the mode is purely index guided, hence showing a nearly linear dispersion. However, the mode is still strongly confined in the PhC waveguide and provides most of the transmission. The dip at 1325nm can be identified as a stop band that arises from the folding of the fundamental mode at the edge of the Brillouin zone. This fundamental mode is crossing the light line at around $0.355c/a$, which explains the appearance of the cutoff at 1235nm. Multiple resonances between 1280nm and 1235nm are arising from the coupling of the fundamental mode with numerous slab modes. Such behavior is very analogous to the mode mixing mechanism observed recently in SOI double-trench waveguides [11]. The spectral region between the stop band at 1325nm and the onset of the resonances at 1280nm is characterized by relatively low-loss propagation. Measurements at 1300nm indicate losses are as small as $16\pm 3\text{dB/cm}$.

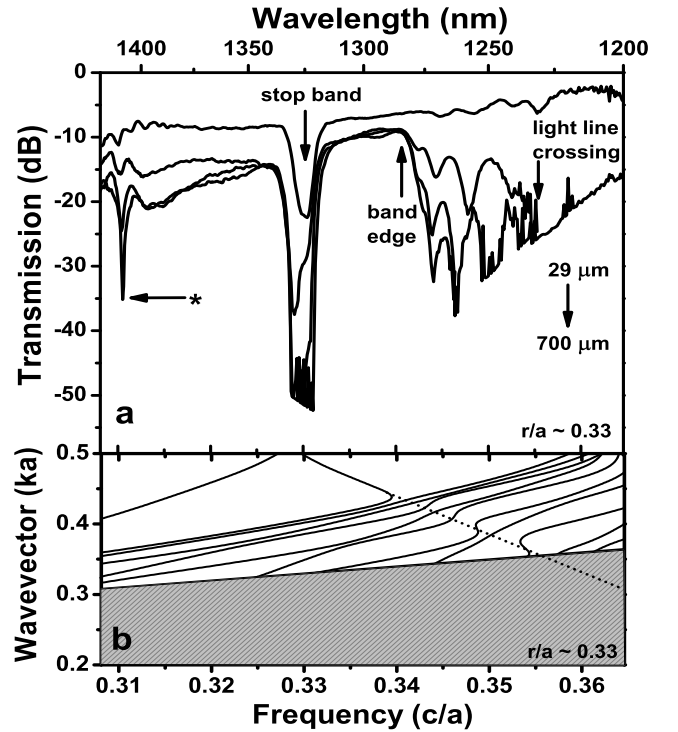


FIG. 6: a) Length series of TM transmission spectra of PhC waveguides ($29-700\mu\text{m}$) with hole radii $r/a\sim 0.33$. The transmission dip marked with an asterisk corresponds to the x -odd TE-like mode (see text for details). b) 3D plane wave band structure calculations. The dotted line indicates the fundamental TM-like waveguiding mode.

loun zone. This fundamental mode is crossing the light line at around $0.355c/a$, which explains the appearance of the cutoff at 1235nm. Multiple resonances between 1280nm and 1235nm are arising from the coupling of the fundamental mode with numerous slab modes. Such behavior is very analogous to the mode mixing mechanism observed recently in SOI double-trench waveguides [11]. The spectral region between the stop band at 1325nm and the onset of the resonances at 1280nm is characterized by relatively low-loss propagation. Measurements at 1300nm indicate losses are as small as $16\pm 3\text{dB/cm}$.

The results of the analyzed TM transmission spectra for hole radii from $r/a=0.32-0.38$ are summarized in Fig. 7. The solid lines are the result of photonic band structure calculations. For the two size series, a slab thickness of $h/a=0.473$ or 0.515 was chosen as an input parameter. These are the same values as for the corresponding TE-like photonic band structures in Fig. 6 and Fig. 1, respectively. The calculations are in good agreement with the experimental results. The inset of Fig. 7 shows the TM spectra of two waveguides, identical in length ($29\mu\text{m}$), but different hole radii ($0.348a$ and $0.371a$). The shift of the transmission spectra for differently chosen hole radii is clearly visible. However, comparison with the corre-

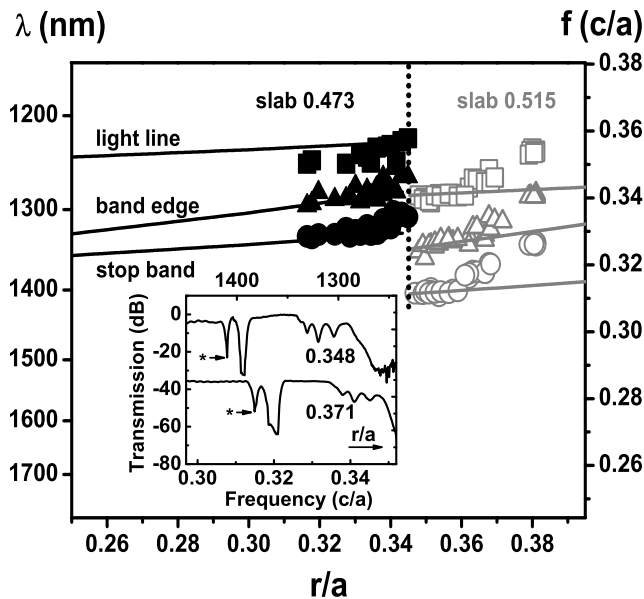


FIG. 7: Experimental TM-map of the spectral positions of light line (squares), band edge (triangles) and stop band (circles) as a function of the hole radius $r/a=0.32-0.38$. Solid lines represent 3D plane wave band structure calculations (black and grey) with input parameters according to the experimental SEM results for hole radii of $r/a=0.32-0.34$ or $r/a=0.35-0.38$ respectively. Inset: TM spectra of two PhC waveguides, identical in length ($29/\mu\text{m}$), but with different hole radii ($0.348a$ and $0.371a$). The transmission dips marked with an asterisk correspond to the x -odd TE-like mode (see text for details).

sponding TE spectra of the identical waveguides (see Fig. 1b) shows that the TM modes exhibit a less pronounced dependence on the hole radius. In contrast to this, comparing the map of TM-like modes in Fig. 7 to the map of TE-like modes in Fig. 5, the spectral shift between the series of different SOI wafers is far more pronounced. Such behavior is not unexpected since TM-like modes are polarized perpendicular to the slab plane and are therefore strongly influenced by a change in the slab thickness and less by the hole radius.

VI. COUPLING BETWEEN EVEN AND ODD MODES

In principle, a W1 SOI waveguide is not single-moded over the entire bandwidth of the PBG. It is known that it can support two TE-like modes (both even with respect to the xy -plane in the slab) possessing different symmetries with respect to the zx -plane vertically bisecting the slab along the waveguide direction (x -axis). All results presented so far correspond to the in-plane x -even TE-like mode. This mode is of most interest for integrated photonics [4, 5, 6, 7, 8, 9, 10, 11, 12, 13, 14]. The TE-like

mode with odd zx -symmetry is visible in all band structure calculations (e.g. Fig. 1a at $c/a=0.31$). However, the excitation of this x -odd TE-like mode with the x -even TE mode in the access strip waveguide is prohibited due to symmetry restrictions. The orthogonality of the x -even and x -odd TE-like modes in the PhC waveguides also prohibits any interaction. Correspondingly, the odd mode is usually not observed in transmission spectra and its properties are regarded as irrelevant to waveguiding in PhC waveguides.

Indeed, in the experimental TE spectra of PhC waveguides with large hole radii (Fig. 1b) no evidence of this mode at 1430nm ($r/a=0.348$) or 1390nm ($r/a=0.379$) is observed. TE transmission spectra of PhC waveguides with small hole radii (Fig. 3b) are also well explained by the photonic band structure and FDTD calculations, as discussed above. However, there is another spectral feature present in these spectra, which does not fit into this picture of forbidden mode coupling. At wavelengths around 1600nm, a distinct break down within the LLP region is observed (marked with an asterisk in Fig. 3b). Its attenuation gradually increases as a function of the PhC waveguide length. As seen from the band structure calculations in Fig. 4b, in this spectral range no other modes except the in-plane x -odd TE-like mode are present. Since no indication of the x -odd TE-like mode is visible in the spectra of short waveguides (Fig. 1b, Fig. 3b), we can conclude that this is not an interface phenomenon but rather the x -even TE-like mode, being excited from the strip waveguide and gradually transferring energy to the x -odd mode. The field energy, once transferred, cannot couple efficiently into the output strip waveguide due to symmetry restrictions and therefore dissipates in the slab. Correspondingly, the x -even TE-like mode exhibits additional propagation losses, which can be estimated from Fig. 3b as 20dB/cm at the center of the dip at around 1600nm. This weak efficiency of mode coupling explains the absence of the x -odd mode in Fig. 1b since the presented PhC waveguides are only $29\mu\text{m}$ in length and the resulting losses would only be $\sim 0.5\text{dB}$. Furthermore, the frequency range where both modes coexist is located far above the light line ($c/a\sim 0.32$ in Fig. 1c) where diffraction losses due to out-of-plane leakage dominate.

In general, the presence of both modes in the experimental spectra indicates that the perfect symmetry of the PhC lattice with respect to zx -plane is somehow relaxed and the interaction between the modes can become possible. Two different mechanisms can in principle be considered that might cause the violation of symmetry in the otherwise highly symmetric (001) plane of the SOI wafer: structural irregularities in the PhC lattice or in-plane optical anisotropy.

Asymmetry in the waveguide can in principle be introduced by structural imperfections of the PhC lattice. Sidewall surface roughness was measured to be only a

few nm [21] and therefore is believed to be an unlikely candidate. Small lateral offsets of the crystal can occur due to imperfect field and sub-field stitching when devices are defined with electron-beam lithography. Offsets in the y -axis would result in an xz -asymmetry of the PhC waveguide and could be a possible cause of mode-mixing. A field (with dimensions of $400\mu\text{m}$) usually has a stitch error $<10\text{-}20\text{nm}$ while sub-fields ($\sim 6\mu\text{m}$) are typically even smaller, however the impact of stitching error requires further systematic investigation. A further possible source of asymmetry is stress in the Si film. While Si is a cubic crystal, and should therefore be optically isotropic, small birefringence ($\Delta n \sim 10^{-6}$) has been reported [22]. Significant birefringence can be induced by stress, and is a known problem for SOI rib waveguides [23]. However, for released Si membranes fabricated on Unibond SOI wafers [24] it is difficult to expect strain higher than a few tens of MPa. Further investigation is necessary to confirm the origin of the observed mode mixing.

Interestingly, the spectral signature of the x -odd TE-like mode can also be identified in TM transmission spectra. For example, the data in Fig. 6a, which shows TM transmission spectra of PhC waveguides with $r/a=0.33$, exhibit a pronounced dip around 1410nm (again marked with an asterisk). Similar dips are also observed in the TM transmission spectra of PhC waveguides of larger hole radii (Inset of Fig. 7). The corresponding photonic band structure of the TM modes in Fig. 6b cannot explain this spectral feature. Instead, its spectral position exactly coincides with the x -odd TE-like mode at the edge of the Brillouin zone at $k=0.5$ (Fig. 1a,c and Fig. 4b).

The spectral positions of these dips in both, TE and TM spectra are plotted in Fig. 8. Data points for $r/a=0.22\text{-}0.24$ are taken from TE spectra and for $r/a=0.32\text{-}0.38$ from TM spectra. The solid line represents the calculated dependency of the x -odd TE-like waveguiding mode on the hole radius for a slab thickness of $h/a=0.473$. In analogy to Fig. 5, the spectral step-like shift between the different size series again follows the change in the slab thickness. Remarkably all data points for both, TE and TM spectra are in good agreement with plane wave calculations for the x -odd TE-like mode over the entire range of hole radii.

Just as for the TE-like transmission spectra, the attenuation at the center of the dip in the TM spectra gradually increases with waveguide length. We can therefore again exclude any significant contribution of energy transfer between the modes already at the interface between the strip waveguide and the PhC. The energy transfer between the TM-like and TE-like x -odd mode is taking place gradually while the light is propagating along the waveguide.

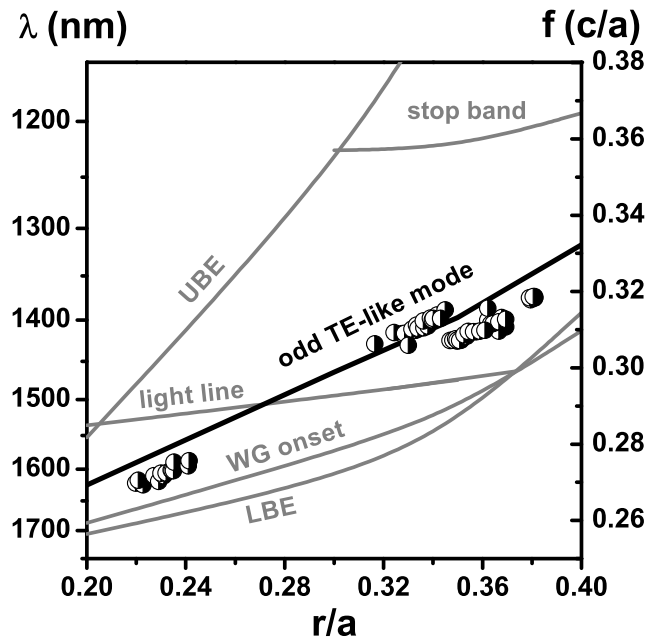


FIG. 8: Experimental map of the x -odd TE-like waveguiding mode as a function of the hole radius. Solid lines represent 3D plane wave band structure calculations with input parameters according to SEM measurements for hole radii of $r/a=0.32\text{-}0.34$. The black line plots the x -odd TE mode while the grey lines represent the UBE, light line, WG onset (even TE mode), stop band and LBE.

VII. SUMMARY

In this paper we have performed an extensive investigation of the transmission properties of SOI-type PhC W1-waveguides as a function of the hole radius, slab thickness and the crystal length for both TE and TM polarizations. Our experimental results reveal that for structural parameters optimized for maximization of the PBG, the bandwidth for low-loss propagation below the light line cutoff completely vanishes for hole radii $r/a > 0.37$. This is mainly caused by a tremendous spectral shift of the lower band edge slab modes, which are mostly localized in the slab surrounding the holes and are strongly influenced by a decrease of the average refractive index of the slab. PhC W1-waveguides with a maximized PBG are therefore unsuitable for integrated photonics applications. The experimental findings for PhC waveguides possessing small holes with only $r/a \sim 0.2$ demonstrate that the bandwidth for transmission can be maximized to almost 130nm while still maintaining a sufficient PBG. Losses for these devices are reduced to only 8dB/cm presumably due to a significantly lower surface area of the holes sidewalls. The experimental transmission spectra for both TE and TM polarizations show very good agreement with calculated photonic band structures and 3D-FDTD transmission spectra.

ACKNOWLEDGMENTS

The authors gratefully acknowledge useful discussions with N. Moll (IBM Zurich Research Lab) and G.L.Bona (IBM Almaden Research lab) and the contributions of the Microelectronics Research Laboratory staff at the IBM T. J. Watson Research Center.

* Corresponding author; e-mail: fdulkei@us.ibm.com

- [1] T. F. Krauss, R. M. De La Rue, and S. Brand, *Nature*, **383**, 699 (1996).
- [2] T. Baba, N. Fukaya, and J. Yonekura, *Electron. Lett.*, **35**, 654 (1999).
- [3] S. Y. Lin, E. Chow, S. G. Johnson, and J. D. Joannopoulos, *Opt. Lett.*, **25**, 1299 (2000).
- [4] T. Baba, N. Fukaya, and A. Motegi, *Electron. Lett.*, **37**, 761 (2001)
- [5] M. Loncar, D. Nedeljkovic, T. Doll, J. Vuckovic, A. Scherer, and T. P. Pearsall, *Appl. Phys. Lett.*, **77**, 1937 (2000).
- [6] M. Loncar, T. Doll, J. Vuckovic, and A. Scherer, *J. Lightwave Technol.*, **18**, 1402 (2000); M. Loncar, D. Nedeljkovic, T. P. Pearsall, J. Vuckovic, A. Scherer, S. Kuchinsky and D. Allan, *Appl. Phys. Lett.*, **80**, 1689 (2002).
- [7] M. Notomi, A. Shinya, K. Yamada, J. Takahashi, and I. Yokohama, *Electron. Lett.*, **37**, 293 (2001).
- [8] M. Notomi, K. Yamada, A. Shinya, J. Takahashi, C. Takahashi, and I. Yokohama, *Phys. Rev. Lett.*, **87**, 253902 (2001).
- [9] W. Bogaerts, V. Wiaux, D. Taillaert, S. Beckx, B. Luyssaert, P. Bienstman, and R. Baets, *IEEE Sel. Top. Quantum Electron.*, **8**, 928 (2002)
- [10] S. J. McNab, N. Moll, and Yu. A. Vlasov, *Opt. Express*, **11**, 2927, 2003.
- [11] Yu. A. Vlasov, N. Moll and S. J. McNab, *Journ. Appl. Phys.*, **95**, 4095 (2004).
- [12] M. Zelsmann, E. Picard, T. Charvolin, E. Hadji, M. Heitzmann, B. Dalzotto, M. E. Nier, C. Seassal, P. Rojo-Romeo, and X. Letartre, *Journ. Appl. Phys.*, **95**, 1606 (2004)
- [13] Y. Sugimoto, Y. Tanaka, N. Ikeda, Y. Nakamura, K. Asakawa and K. Inoue, *Opt. Express*, **12**, 1090 (2004).
- [14] M. Notomi, A. Shinya, S. Mitsugi, E. Kuramochi, and H-Y Ryu, *Opt. Express*, **12**, 1551 (2004)
- [15] S. G. Johnson, S. Fan, P. R. Villeneuve, J. D. Joannopoulos, L. A. Kolodziejski, *Phys. Rev. B* **60**, 5751 (1999).
- [16] S. G. Johnson, P. R. Villeneuve, S. Fan, and J. D. Joannopoulos, *Phys. Rev. B*, **62**, 8212, 2000.
- [17] A. Chutinan and S. Noda, *Phys. Rev. B*, **62**, 4488 (2000).
- [18] E. Chow, S. Y. Lin, S. G. Johnson, P. R. Villeneuve, J. D. Joannopoulos, J. R. Wendt, G. A. Vawter, W. Zubrzycki, H. Hou, and A. Alleman, *Nature*, **407**, 983 (2000).
- [19] S. G. Johnson and J. D. Joannopoulos, *Opt. Express* **8**, 173 (2001).
- [20] Rsoft Design Group, *Fullwave 4.0 Manual* (2005).
- [21] Yu. A. Vlasov and S. J. McNab, *Opt. Express* **12**, 1622 (2004).
- [22] J. Pastrnak, K. Vedam *Phys. Rev. B* **3**, 2567 (1971).
- [23] see for example D.-X. Xu et al. *Optics Lett.* **29**, 2384 (2004).
- [24] G. K. Celler, S. Cristoloveanu, *Journ. Appl. Phys.*, **93**, 4955 (2003).